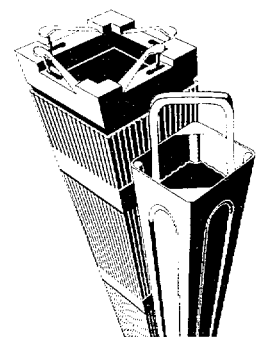


SIEMENS

EMF-2209(NP)
Revision 1

SPCB Critical Power Correlation

March 2000



Siemens Power Corporation
Nuclear Division

Siemens Power Corporation

ISSUED IN SPC ON-LINE
DOCUMENT SYSTEM
DATE: 3/21/00

EMF-2209(NP)
Revision 1

Issue Date:

SPCB Critical Power Correlation

Prepared:

R. B. Macduff
R. B. Macduff, Staff Engineer
Safety Analysis Methods

17 Mar 2000
Date

Prepared:

T. H. Keheley
T. H. Keheley, Staff Engineer
Safety Analysis Methods

Date

/lmk

**U.S. Nuclear Regulatory Commission
Report Disclaimer**

Important Notice Regarding Contents and Use of This Document

Please Read Carefully

This technical report was derived through research and development programs sponsored by Siemens Power Corporation. It is being submitted by Siemens Power Corporation to the U.S. Nuclear Regulatory Commission as part of a technical contribution to facilitate safety analyses by licensees of the U.S. Nuclear Regulatory Commission which utilize Siemens Power Corporation fabricated reload fuel or technical services provided by Siemens Power Corporation for light water power reactors and it is true and correct to the best of Siemens Power Corporation's knowledge, information, and belief. The information contained herein may be used by the U.S. Nuclear Regulatory Commission in its review of this report and, under the terms of the respective agreements, by licensees or applicants before the U.S. Nuclear Regulatory Commission which are customers of Siemens Power Corporation in their demonstration of compliance with the U.S. Nuclear Regulatory Commission's regulations.

Siemens Power Corporation's warranties and representations concerning the subject matter of this document are those set forth in the agreement between Siemens Power Corporation and the Customer pursuant to which this document is issued. Accordingly, except as otherwise expressly provided in such agreement, neither Siemens Power Corporation nor any person acting on its behalf:

- a. makes any warranty, or representation, express or implied, with respect to the accuracy, completeness, or usefulness of the information contained in this document, or that the use of any information, apparatus, method, or process disclosed in this document will not infringe privately owned rights;

or

- b. assumes any liabilities with respect to the use of, or for damages resulting from the use of, any information, apparatus, method, or process disclosed in this document.

SPCB Critical Power Correlation

Reviewed: *ASR*
D. S. Rowe
Rowe & Associates
Date _____

Concurred: *ASR*
R. E. Collingham, Manager
Safety Analysis Methods
Date _____

Approved: *ASR*
R. L. Feuerbacher, Vice President
Engineering
Date _____

Approved: *J. F. Mallay*
J. F. Mallay, Director
Regulatory Affairs
Date 3/21/00

Nature of Changes

Item	Page(s)	Description and Justification
1.	1-3	Deleted sentence below Table 1.2. <u>Justification:</u> Sentence determined to be unnecessary.
2.	2-4	Corrected A3** to A3* in Equation 2.7 and replaced G with \bar{G} in Tables 2.1 and 2.2. <u>Justification:</u> Correction
3.	2-5 through 2-7	Replaced G with \bar{G} in tables. <u>Justification:</u> Correction
4.	2-23	Corrected reference from Reference 2.1 to Reference 2.2. <u>Justification:</u> Correction
5.	2-26	Inserted legend for test pressures in revised Figure 2.3. <u>Justification:</u> Requested by NRC reviewer.
6.	2-34	Changed reference to ANFB to SPCB in last sentence of 2.6.1.2. <u>Justification:</u> Correction
7.	3-1 and 3-2	Inserted revised Tables 3.1 and 3.2 and changed note and title to Table 3.2. <u>Justification:</u> Requested by NRC reviewer.
8.	3-3	Inserted corrected numbers for m_2 , $\sqrt{\beta_1}$, and β_2 . <u>Justification:</u> Correction
9.	3-4 through 3-29	Modified title of figures to include number of data. <u>Justification:</u> Requested by NRC reviewer.
10.	4-2	Inserted revised Tables 4.1 and 4.2 to expand the tabular information. <u>Justification:</u> Revised as requested by NRC reviewer.
11.	4-4	Revised Table 4.3 to expand tabular information and moved to page 4-5. <u>Justification:</u> Revised as requested by NRC reviewer.
12.	4-5 through 4-17	Changed pagination due to insertion of larger Table 4.3. <u>Justification:</u> Update
13.	5-14	Referenced Table 5.5 rather than Table 5.9. <u>Justification:</u> Correction

Contents

1.	Introduction and Summary	1-1
1.1	SPCB Data Base	1-2
1.2	SPCB Comparison to the Data Base	1-3
1.3	References	1-5
2.	SPCB Correlation.....	2-1
2.1	SPCB Base Correlation	2-2
2.1.1	Functions of A and B	2-3
2.1.2	Function C - ATRIUM-9B	2-5
2.1.3	Function C - ATRIUM-10	2-6
2.2	Non-Uniform Axial Heat Flux Factor	2-7
2.2.1	Non-Uniform Factor Corrector	2-8
2.2.2	Gradient Function	2-10
2.3	Radial Heat Flux Distribution (Rod Centered Local Peaking Function)	2-13
2.3.1	FEFFO for Corner Rods	2-14
2.3.2	FEFFO for Side Rods	2-15
2.3.3	FEFFO for Interior Rods	2-17
2.3.4	FEFFO for Interior Rods Adjacent to the ATRIUM Water Canister	2-19
2.3.5	Weighting Factors	2-22
2.3.6	Bundle Geometry/Spacer Effects (Additive Constants)	2-23
2.4	SPCB Correlation Behavior	2-24
2.4.1	Functional Behavior of Major Functions Within SPCB	2-25
2.4.2	Overall Behavior of SPCB	2-26
2.5	Additive Constants	2-32
2.6	Correlation Range and Applicability	2-33
2.6.1	Mass Velocity	2-33
2.6.2	Enthalpy	2-35
2.6.3	Pressure	2-37
2.6.4	Inlet Subcooling	2-37
2.7	SPCB Application to Other Fuel Designs	2-37
2.8	References	2-37
3.	Statistical Analysis of SPCB Critical Power Data	3-1
3.1	SPCB Descriptive Statistics	3-1
3.2	Statistical Tests	3-5
3.3	SPCB Correlation Behavior	3-5
3.4	Statistics by Subgroups	3-8
3.4.1	Mass Flow Rate	3-8
3.4.2	Pressure	3-9
3.4.3	Enthalpy at Boiling Transition	3-9
3.4.4	FEFF	3-10
3.4.5	Axial Offset	3-11
3.4.6	Mass Flow Rate and Test Section	3-11
3.4.7	Mass Flow Rate and Enthalpy Groups	3-13

3.5 ECPR - Mass Flow Plots	3-14
3.6 Additive Constant Statistics.....	3-29
3.6.1 Additive Constant Determination	3-30
3.6.2 Additive Constant Uncertainty.....	3-33
3.6.3 High Local Peaking.....	3-36
3.6.4 SPCB Conservatism.....	3-39
3.7 SPCB Predictions Compared with Measurements	3-40
3.8 References	3-41
4. Correlation Validation	4-1
4.1 Assessment of ATRIUM-9B/ATRIUM-10 Critical Power Data.....	4-1
4.1.1 Comparison of ATRIUM-9B Verification and Validation Data.....	4-1
4.1.2 Comparison ATRIUM-10 Verification and Validation Data	4-4
4.2 Validation with Alternate Design.....	4-7
4.3 Evaluation of Transient Critical Power Data	4-9
4.3.1 Conclusions	4-16
4.4 References	4-17
5. SPCB Data Base.....	5-1
5.1 Facility Description	5-1
5.2 Test Bundle Descriptions	5-2
5.2.1 ATRIUM-9B	5-2
5.2.2 ATRIUM-10	5-3
5.3 Test Strategy	5-11
5.3.1 Radial Peaking Profiles.....	5-11
5.3.2 Axial Power Profile.....	5-12
5.3.3 Thermal Hydraulic Test Conditions.....	5-13
5.3.4 Test Design	5-13
5.4 SPCB Data.....	5-14
5.5 References	5-169

Tables

Table 1.1 SPCB Range of Applicability	1-2
Table 1.2 Enthalpy Bounds for SPCB.....	1-3
Table 2.1 Coefficients for A.....	2-4
Table 2.2 Coefficients of B	2-4
Table 2.3 ATRIUM-9B Coefficients for C.....	2-5
Table 2.4 Coefficient Dependence on Mass Velocity.....	2-6
Table 2.5 ATRIUM-10 Coefficients for C	2-7
Table 2.6 CORPR Coefficients.....	2-9
Table 2.7 CORPAT10 Coefficients.....	2-10
Table 3.1 Critical Power Ratio Statistics for SPCB Correlation.....	3-1
Table 3.2 Descriptive Statistics.....	3-2
Table 3.3 Inlet Mass Flow Rate Statistics	3-9
Table 3.4 Pressure Statistics.....	3-9
Table 3.5 Boiling Transition Enthalpy Statistics	3-10
Table 3.6 FEFF Statistics	3-10
Table 3.7 Axial Offset Statistics.....	3-11
Table 3.8 Test Section and Flow Statistics.....	3-11
Table 3.9 Flow and Inlet Subcooling Statistics	3-13
Table 3.10 SPCB Additive Constants - ATRIUM™-9B	3-29
Table 3.11 SPCB Additive Constants - ATRIUM™-10.....	3-30
Table 3.12 Summary of Rods in Boiling Transition.....	3-31
Table 3.13 Test Section FEFFBT Values and Standard Deviations.....	3-32
Table 3.14 Composite Values of FEFFBT	3-35
Table 3.15 Additional Additive Constant Uncertainty for High Local Peakings.....	3-39
Table 3.16 FEFF Values for ECPR Evaluation	3-39
Table 4.1 ATRIUM-9B Comparison (Verification/Validation).....	4-2
Table 4.2 Additional Validation	4-2
Table 4.3 ATRIUM-10 Comparison	4-5
Table 4.4 Transient Initial Conditions	4-14
Table 4.5 XCOBRA-T Results Using Nominal F-eff.....	4-15
Table 5.1 Test Loop Uncertainties.....	5-10
Table 5.2 Physical Characteristics of the ATRIUM-9B Test Assembly	5-10
Table 5.3 Physical Characteristics of the ATRIUM-10 Test Assembly.....	5-10
Table 5.4 Dryout Test Data	5-13
Table 5.5 SPCB Data and Analysis Results	5-15

Figures

Figure 1.1 Comparison of Predicted and Measured Critical Power with SPCB for ATRIUM™-9B Data	1-4
Figure 1.2 Comparison of Predicted and Measured Critical Power Data with SPCB for ATRIUM™-10 Data	1-5
Figure 2.1 Function A	2-25
Figure 2.2 Function B	2-25
Figure 2.3 Function (1-B/G)	2-26
Figure 2.4 SPCB Critical Power vs Flow Rate for ATRIUM-10	2-27
Figure 2.5 SPCB Critical Power vs Flow Rate for ATRIUM-9B	2-27
Figure 2.6 SPCB Critical Power Variation with Pressure for ATRIUM-10	2-28
Figure 2.7 SPCB Critical Power Variation with	2-28
Figure 2.8 SPCB Critical Power Variation with Inlet	2-29
Figure 2.9 SPCB Critical Power Variation with Inlet	2-29
Figure 2.10 SPCB Critical Power Variation with FEFF for ATRIUM-10	2-30
Figure 2.11 SPCB Critical Power Variation with FEFF for ATRIUM-9B	2-30
Figure 2.12 Axial Power Shapes for SPCB Sensitivity	2-31
Figure 2.13 SPCB Critical Power Variation with Axial Power Profiles for ATRIUM-10	2-32
Figure 2.14 SPCB Critical Power Variation with Axial Power Profiles for ATRIUM-9B	2-32
Figure 3.1 Distribution of Critical Power Ratio Using SPCB for 2657 Data	3-4
Figure 3.2 Normality Plot for SPCB for 2657 Data	3-5
Figure 3.3 SPCB ECPR versus Local Mass Flow Rate for 2657 Data	3-6
Figure 3.4 SPCB ECPR versus Boiling Transition Enthalpy for 2657 Data	3-6
Figure 3.5 SPCB ECPR versus Pressure for 2657 Data	3-7
Figure 3.6 SPCB ECPR versus Assembly FEFF for 2657 Data	3-7
Figure 3.7 SPCB ECPR Versus Axial Offset for 2657 Data	3-8
Figure 3.8 ECPR Versus Mass Flow Rate, ATRIUM-9B with SPCB for 42 Data	3-15
Figure 3.9 ECPR Versus Mass Flow Rate, ATRIUM-9B with SPCB for 41 Data	3-15
Figure 3.10 ECPR Versus Mass Flow Rate, ATRIUM-9B with SPCB for 42 Data	3-16
Figure 3.11 ECPR Versus Mass Flow Rate, ATRIUM-9B with SPCB for 288 Data	3-16
Figure 3.12 ECPR Versus Mass Flow Rate, ATRIUM-9B with SPCB for 297 Data	3-17
Figure 3.13 ECPR Versus Mass Flow Rate, ATRIUM-9B with SPCB for 309 Data	3-17
Figure 3.14 ECPR Versus Mass Flow Rate, ATRIUM-9B with SPCB for 322 Data	3-18
Figure 3.15 ECPR Versus Mass Flow Rate, ATRIUM-9B with SPCB for 44 Data	3-18
Figure 3.16 ECPR Versus Mass Flow Rate, ATRIUM-9B with SPCB for 244 Data	3-19
Figure 3.17 ECPR Versus Mass Flow Rate, ATRIUM-10 with SPCB for 37 Data	3-19
Figure 3.18 ECPR Versus Mass Flow Rate, ATRIUM-10 with SPCB for 31 Data	3-20
Figure 3.19 ECPR Versus Mass Flow Rate, ATRIUM-10 with SPCB for 32 Data	3-20
Figure 3.20 ECPR Versus Mass Flow Rate, ATRIUM-10 with SPCB for 43 Data	3-21
Figure 3.21 ECPR Versus Mass Flow Rate, ATRIUM-10 with SPCB for 34 Data	3-21
Figure 3.22 ECPR Versus Mass Flow Rate, ATRIUM-10 with SPCB for 44 Data	3-22
Figure 3.23 ECPR Versus Mass Flow Rate, ATRIUM-10 with SPCB for 38 Data	3-22
Figure 3.24 ECPR Versus Mass Flow Rate, ATRIUM-10 with SPCB for 117 Data	3-23
Figure 3.25 ECPR Versus Mass Flow Rate, ATRIUM-10 with SPCB for 23 Data	3-23
Figure 3.26 ECPR Versus Mass Flow Rate, ATRIUM-10 with SPCB for 39 Data	3-24

Figure 3.27 ECPR Versus Mass Flow Rate, ATRIUM-10 with SPCB for 34 Data	3-24
Figure 3.28 ECPR Versus Mass Flow Rate, ATRIUM-10 with SPCB for 49 Data	3-25
Figure 3.29 ECPR Versus Mass Flow Rate, ATRIUM-10 with SPCB for 44 Data	3-25
Figure 3.30 ECPR Versus Mass Flow Rate, ATRIUM-10 with SPCB for 47 Data	3-26
Figure 3.31 ECPR Versus Mass Flow Rate, ATRIUM-10 with SPCB for 42 Data	3-26
Figure 3.32 ECPR Versus Mass Flow Rate, ATRIUM-10 with SPCB for 95 Data	3-27
Figure 3.33 ECPR Versus Mass Flow Rate, ATRIUM-10 with SPCB for 102 Data	3-27
Figure 3.34 ECPR Versus Mass Flow Rate, ATRIUM-10 with SPCB for 98 Data	3-28
Figure 3.35 ECPR Versus Mass Flow Rate, ATRIUM-10 with SPCB for 79 Data	3-28
Figure 3.36 ECPR Versus Mass Flow Rate, Upskew Axial Tests with SPCB for 678 Data	3-29
Figure 3.37 Comparison of STS-40.1 and 33.1	3-37
Figure 3.38 Comparison of STS-32.1, 17.5 and 17.6	3-38
Figure 3.39 Comparison of Predicted and Measured Critical Power with SPCB	3-41
Figure 4.1 ATRIUM-9B Validation Data	4-3
Figure 4.2 ATRIUM-9B Validation ECPR Characteristics with Flow	4-4
Figure 4.3 ATRIUM-10 Validation Data	4-6
Figure 4.4 ATRIUM-10 Validation ECPR Characteristics with Flow	4-7
Figure 4.5 ATRIUM-10P Validation Data	4-8
Figure 4.6 Comparison of SPCB with ATRIUM-10P Data	4-9
Figure 4.7 Steady-state Critical Power versus Inlet Flow for Tests 17.8 and 29.5 at Inlet Subcooling of 20 Btu/lbm	4-10
Figure 4.8 Typical Pressurization Transient Forcing Function	4-11
Figure 4.9 Typical Flow Decay Transient Forcing Function	4-12
Figure 4.10 Thermocouple Response for Typical Transient Test	4-13
Figure 4.11 Comparison of Measured and Calculated Time of Boiling Transition	4-16
Figure 5.1 Karlstein Thermal Hydraulic Test Loop	5-5
Figure 5.2 Test Vessel	5-6
Figure 5.3 Thermocouple Locations	5-7
Figure 5.4 Bundle Spacer Locations	5-8
Figure 5.5 Rod Axial Power Profiles Tested	5-9
Figure 5.6 Peaking Pattern STS 12.1. Dryout detections indicated by heavy outline	5-85
Figure 5.7 STS 12.1	5-86
Figure 5.8 Peaking Pattern STS 12.2. Dryout detections indicated by heavy outline	5-87
Figure 5.9 STS 12.2	5-88
Figure 5.10 Peaking Pattern STS 12.3. Dryout detections indicated by heavy outline	5-89
Figure 5.11 STS 12.3	5-90
Figure 5.12 Peaking Pattern STS 33.1. Dryout detections indicated by heavy outline	5-91
Figure 5.13 STS 33.1 - 600 psi	5-92
Figure 5.14 STS 33, 800 psi	5-93
Figure 5.15 STS 33, 1000 psi	5-94
Figure 5.16 STS 33, 1200 psi	5-95
Figure 5.17 STS 33, 1400 psi	5-96
Figure 5.18 Peaking Pattern STS 34.1. Dryout detections indicated by heavy outline	5-97

Figure 5.19	STS 34, 600 psi.....	5-98
Figure 5.20	STS 34, 800 psi.....	5-99
Figure 5.21	STS 34, 1000 psi.....	5-100
Figure 5.22	STS 34, 1200 psi.....	5-101
Figure 5.23	STS 34, 1400 psi.....	5-102
Figure 5.24	Peaking Pattern STS 35.1. Dryout detections indicated by heavy outline.....	5-103
Figure 5.25	STS 35, 600 psi.....	5-104
Figure 5.26	STS 35, 800 psi.....	5-105
Figure 5.27	STS 35, 1000 psi.....	5-106
Figure 5.28	STS 35, 1200 psi.....	5-107
Figure 5.29	STS 35, 1400 psi.....	5-108
Figure 5.30	Peaking Pattern STS 37.1. Dryout detections indicated by heavy outline.....	5-109
Figure 5.31	STS 37, 600 psi.....	5-110
Figure 5.32	STS 37, 800 psi.....	5-111
Figure 5.33	STS 37, 1000 psi.....	5-112
Figure 5.34	STS 37, 1200 psi.....	5-113
Figure 5.35	STS 37, 1400 psi.....	5-114
Figure 5.36	Peaking Pattern STS 38.3. Dryout detections indicated by heavy outline.....	5-115
Figure 5.37	STS 38.....	5-116
Figure 5.38	Peaking Pattern STS 40.1. Dryout detections indicated by heavy outline.....	5-117
Figure 5.39	STS 40, 800 psi.....	5-118
Figure 5.40	STS 40, 1000 psi.....	5-119
Figure 5.41	STS 40, 1200 psi.....	5-120
Figure 5.42	Peaking Pattern STS 17.1. Dryout detections indicated by heavy outline.....	5-121
Figure 5.43	STS 17.1.....	5-122
Figure 5.44	Peaking Pattern STS 17.2. Dryout detections indicated by heavy outline.....	5-123
Figure 5.45	STS 17.2.....	5-124
Figure 5.46	Peaking Pattern STS 17.3. Dryout detections indicated by heavy outline.....	5-125
Figure 5.47	STS 17.3.....	5-126
Figure 5.48	Peaking Pattern STS 17.4. Dryout detections indicated by heavy outline.....	5-127
Figure 5.49	STS 17.4.....	5-128
Figure 5.50	Peaking Pattern STS 17.5. Dryout detections indicated by heavy outline.....	5-129
Figure 5.51	STS 17.5.....	5-130
Figure 5.52	Peaking Pattern STS 17.6. Dryout detections indicated by heavy outline.....	5-131
Figure 5.53	STS 17.6.....	5-132
Figure 5.54	Peaking Pattern STS 17.7. Dryout detections indicated by heavy outline.....	5-133
Figure 5.55	STS 17.7.....	5-134
Figure 5.56	Peaking Pattern STS 17.8. Dryout detections indicated by heavy outline.....	5-135
Figure 5.57	STS 17.8, Low Pressure.....	5-136
Figure 5.58	STS 17.8, 1000 psi.....	5-137
Figure 5.59	STS 17.8, High Pressure.....	5-138
Figure 5.60	Peaking Pattern STS 17.9. Dryout detections indicated by heavy outline.....	5-139
Figure 5.61	STS 17.9.....	5-140
Figure 5.62	Peaking Pattern STS 17.10. Dryout detections indicated by heavy outline.....	5-141
Figure 5.63	STS 17.10.....	5-142
Figure 5.64	Peaking Pattern STS 17.11. Dryout detections indicated by heavy outline.....	5-143
Figure 5.65	STS 17.11.....	5-144
Figure 5.66	Peaking Pattern STS 17.12. Dryout detections indicated by heavy outline.....	5-145
Figure 5.67	STS 17.12.....	5-146

Figure 5.68 Peaking Pattern STS 28.1. Dryout detections indicated by heavy outline.....	5-147
Figure 5.69 STS 28.1	5-148
Figure 5.70 Peaking Pattern STS 28.2. Dryout detections indicated by heavy outline.....	5-149
Figure 5.71 STS 28.2	5-150
Figure 5.72 Peaking Pattern STS 29.1. Dryout detections indicated by heavy outline.....	5-151
Figure 5.73 STS 29.1	5-152
Figure 5.74 Peaking Pattern STS 29.2. Dryout detections indicated by heavy outline.....	5-153
Figure 5.75 STS 29.2, 600 psi.....	5-154
Figure 5.76 STS 29.2, 1000 psi.....	5-155
Figure 5.77 STS 29.2, 1400 psi.....	5-156
Figure 5.78 Peaking Pattern STS 29.4. Dryout detections indicated by heavy outline.....	5-157
Figure 5.79 STS 29.4, 600 psi.....	5-158
Figure 5.80 STS 29.4, 1000 psi.....	5-159
Figure 5.81 STS 29.4, 1400 psi.....	5-160
Figure 5.82 Peaking Pattern STS 29.5. Dryout detections indicated by heavy outline.....	5-161
Figure 5.83 STS 29.5, 600 psi.....	5-162
Figure 5.84 STS 29.5, 1000 psi.....	5-163
Figure 5.85 STS 29.5, 1400 psi.....	5-164
Figure 5.86 Peaking Pattern STS 32.1. Dryout detections indicated by heavy outline.....	5-165
Figure 5.87 STS 32.1, 600 psi.....	5-166
Figure 5.88 STS 32.1, 1000 psi.....	5-167
Figure 5.89 STS 32.1, 1400 psi.....	5-168

1.1 SPCB Data Base

The SPCB data base is comprised of [] steady-state data points taken on [] different test assemblies. The axial power shapes of the tests were [] peak-to-average cosine and [] peak-to-average upskew and downskew. The data base was compiled from tests performed exclusively at the Siemens thermal hydraulic test facility at Karlstein, Germany.

During the correlation development, the data base was divided into a correlating (verification) set of data and a validation data set. Of the [] steady-state data points, [] were set aside for validation. In addition, another [] validation points taken from steady-state critical power tests not included in the data base were analyzed. Transient tests were performed on an ATRIUM-10 test assembly with both a cosine and upskew axial power distribution as part of the correlation validation.

The dryout tests were designed to represent the range of local conditions present in an operating BWR fuel assembly. The data base and correlation address the effects due to operating pressure, mass velocity, enthalpy, axial power profile, and local peaking distribution. Tables 1.1 represents the range of parameters tested. [

] Bounding values for enthalpy are checked at the plane of boiling transition based on ranges shown in Table 1.2.

Table 1.1 SPCB Range of Applicability

Pressure (psia)	571.4 to 1432.2
Inlet Mass Velocity (Mlb/hr-ft ²)	0.087 to 1.5
Inlet Subcooling (Btu/lbm)	5.55 to 148.67
Design Local Peaking	1.5
Tested Local Peaking	1.45

1.2 ***SPCB Comparison to the Data Base***

SPCB has been used to predict the critical power for each data point in the data base. The ratio of the predicted critical power to the measured critical power (Experimental Critical Power Ratio, ECPR) has been determined for each test point and the additional validation points and is used along with the standard deviation of the ECPR as the basis to determine the ability of the correlation to predict critical power. Comparisons of the predicted and measured critical power for both the ATRIUM-9B and the ATRIUM-10 are shown in Figures 1.1 and 1.2, respectively.





1.3 **References**

- 1.1 ANF-1125(P)(A) and Supplements 1 and 2, *ANFB Critical Power Correlation*, Advanced Nuclear Fuels Corporation, April 1990.

2. SPCB Correlation

A BWR fuel assembly operates into the annular flow regime. A liquid film on the rod and a steam-water mixture in the center region characterizes this regime. As the flow progresses upward the water film changes because of boiling off and the deposition of water droplets onto the liquid film. A rapid temperature excursion occurs when the liquid film goes to zero thickness. The loss of this liquid film is variously termed dryout, boiling transition, and critical heat flux (CHF).

The SPCB correlation is similar to the ANFB-10 Critical Power Correlation (Reference 2.1) and the ANFB Critical Power Correlation (Reference 2.2). All three correlations use empirical fits to the data that use planar average conditions to predict critical heat flux. The form of the correlations is that developed by Macbeth (Reference 2.3). This correlation form is developed by the transformation from the linear behavior of CHF with inlet subcooling to the linear behavior of CHF with local enthalpy. A plot of inlet subcooling versus critical heat flux (for example, see Figure 2.8) shows that critical heat flux varies linearly with inlet subcooling. For uniform heat flux (Base), this relationship can be expressed

$$q''_{\text{Base}} = A + B(h_{\text{in}}) \quad (2.1)$$

where A and B are functions of pressure and flow and h_{in} is the inlet subcooling. However, inlet enthalpy is not an appropriate parameter for a transient application, so the correlation must be converted for local conditions by application of a channel average heat balance. This results in the form

$$q''_{\text{Base}} = \frac{A - B(h_{\text{bt}})}{1 - \frac{B}{G}} \quad (2.2)$$

where G is the mass velocity and h_{bt} is the enthalpy at the plane of boiling transition. For the SPCB application another term, C, is added to h_{bt} . This parameter is specific to the fuel type being analyzed. Also non-uniform axial power corrector is used which is developed from the

Tong factor (Reference 2.3) used in the analysis of BWR core thermal-hydraulic behavior. This corrector is based on a mass balance on the liquid film and has the form

$$F = \frac{\Omega}{q''_{\ell_c} (1 - e^{-\Omega \ell_c})} \int_0^{\ell_c} \left[e^{-\Omega(\ell_c - Z)} \right] q''(Z) dZ \quad (2.3)$$

In this expression, Ω is a function of mass velocity and heat flux gradient, $q''(Z)$ is the axial heat flux, ℓ_c is the axial plane of interest, and Z is the position on the fuel rod. [

]

Combining equations 2.2 and 2.3 results in the correlation for a non-uniform (NU) heat flux case,

$$q''_{NU} = \frac{q''_{Base}}{F} \quad (2.4)$$

This formulation is the basis for the SPCB correlation.

2.1 **SPCB Base Correlation**

Using the Macbeth form of the critical heat flux equation developed above, SPCB Correlation has the following form:



2.1.1 Functions of A and B

The terms A and B are applicable to both the ATRIUM-9B and ATRIUM-10. The functions A and B have the form







2.2 *Non-Uniform Axial Heat Flux Factor*

The non-uniform axial power corrector (Tong et al., Reference 2.3) used in the ANFB critical power correlation (Reference 2.2) provides the basis of the non-uniform axial correction factor for SPCB. The non-uniform axial correction factor characteristic modified in SPCB is the empirical factor, " Ω " (Reference 2.4). In addition, a post-multiplier to the non-uniform axial factor is included to provide an adjustment to better address the impact of non-uniform axial shapes. This adjustment factor is appropriate for the steady-state and transient evaluation processes. [

]

The base non-uniform axial factor is given by:

$$F_{\text{Base}} = \frac{\Omega}{q''_{\ell_c} (1 - e^{-\Omega \ell_c})} \int_0^{\ell_c} \left[e^{-\Omega(\ell_c - Z)} \right] q''(Z) dZ \quad (2.14)$$

where

- $q''(Z)$ = Axial heat flux
- Z = Axial position on fuel rod
- Ω^a = Empirical factor (described below)
- ℓ_c = Axial position of plane of interest

2.2.1 Non-Uniform Factor Corrector

An additional correction is obtained by multiplying the base non-uniform axial factor, F_{Base} , by the following pressure, flow, and enthalpy gradient term.

$$[\quad]$$

^a Ω is taken as the [

^b []

^c []



^a [
^b [

]

]

2.2.2 Gradient Function

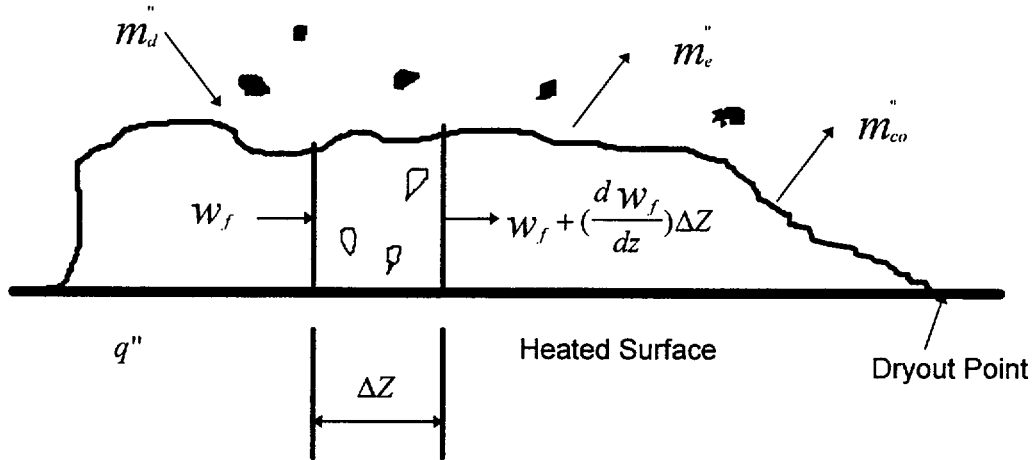
This section describes the GRAD1^a term and how it is calculated and used in evaluating critical power. A gradient type of term was suggested as being important for dryout in References 2.4 and 2.5.

The influence of the axial heat flux shape is effected by the gradient of enthalpy at the location of interest. More specifically, for a steady-state configuration, the gradient of the axial heat flux shape represents the feature being modeled. Enthalpy is used to transform the heat flux shape gradient behavior to the fluid properties used to predict critical heat flux.

^a [

]

It is an experimentally determined fact that dryout normally occurs in a region of decreasing heat flux. This is shown by (see Reference 2.5)



- Let w_f = liquid flow rate
 P_H = heated perimeter
 m_e'' = liquid entrainment mass flux
 m_{co}'' = liquid carryover mass flux
 m_d'' = liquid disposition mass flux
 A_{x-s} = cross section flow area
 W_{le} = entrained liquid flow rate

$$w_f + \frac{dw_f}{dz} \Delta Z + \frac{P_H \Delta Z q''}{h_{fg}} + m_e'' P_H \Delta Z + m_{co}'' P_H \Delta Z - w_f - m_d'' P_H \Delta Z = 0$$

$$\frac{dw_f}{dz} = P_H \left(m_d'' - \frac{q''}{h_{fg}} - m_e'' - m_{co}'' \right)$$

$$w_f = GA_{x-s} (1 - \langle x \rangle) - W_{le}$$

(2.19)

If one assumes that the occurrence of dryout happens when the film flow gradient is zero, then

$$\begin{aligned}\frac{dw_f}{dZ} &= 0 \\ q_c'' &= h_{fg}(m_d'' - m_e'' - m_{co}'') \\ m_e'' &= m_{co}'' = 0 \\ q_c'' &= h_{fg}m_d''\end{aligned}\tag{2.20}$$

Therefore, the spatial derivation of the flow gradient is:

$$\frac{d^2w_f}{dZ^2} = P_H \left(\frac{dm_d''}{dZ} - \frac{1}{h_{fg}} \frac{dq''}{dZ} \right) > 0\tag{2.21}$$

Normally, $\frac{dm_d''}{dZ} < 0$ as dryout is approached since the amount of liquid is decreasing.

Therefore, $\frac{dq''}{dZ} < 0$ for upstream dryout to occur.

The correlation uses the gradient in the evaluation of the post-multiplier to the non-uniform axial factor, as expressed earlier. The value of gradient is determined for every node. The gradient is based on the Equation 2.22.

$$\text{Grad1} = f \left(\frac{\partial^2 h}{\partial z^2} \right)\tag{2.22}$$

where

h represents the enthalpy (Btu/lbm) at node j

z represents the axial elevation (ft) at node j

[

]

[

]

2.3 *Radial Heat Flux Distribution (Rod Centered Local Peaking Function)*

The function C in Equation 2.2 includes the parameter FEFF. The FEFF parameter characterizes the local peaking factor effect on the bundle critical power and is retained from Reference 2.1 and 2.2 and is defined in the same manner. This section describes how the FEFF calculation is applied to ATRIUM-10 and ATRIUM-9B fuel assemblies. The critical power varies inversely with FEFF. That is, as FEFF increases in value, the critical power decreases in value. FEFF has two parts. One part depends solely on the peaking factors of the rod of interest and its immediate neighbors. The other is termed an Additive Constant, ℓ , which accounts for other local effects from spacing and geometry. The Additive Constant is determined from the experimental data. The definitions of FEFF and examples for several rod locations, including rods located adjacent to part-length rods as would be observed for ATRIUM-10 are discussed below.

The portion of FEFF that depends on local peaking distribution is termed FEFFO. FEFFO for the i^{th} rod is calculated from the equation



2.3.1 FEFFO for Corner Rods

Corner rods in a lower lattice of an assembly are adjacent to three fueled rods. This is illustrated as



2.3.2 FEFFO for Side Rods

Side rods could be adjacent to fueled rods and are illustrated as



Similarly, with the unheated portion in a k position, Equation 2.26 becomes



2.3.3 FEFFO for Interior Rods

Interior rods in lower lattices of an ATRIUM-10 fuel assembly are adjacent to other heated rods. In the lattice that considers the plenum of the part-length rod, one rod position is treated as unheated. In the lattice above the top of the part-length rod, one rod position continues to be treated as unheated. Interior rods adjacent to the ATRIUM water canister are addressed in Section 2.3.4.

The rod configuration examined for an interior rod is illustrated as

$$\begin{array}{ccccc} k & & j & & k \\ & j & & i & & j \\ k & & j & & k \end{array}$$

The application of Equation 2.23 for rod i becomes





[

]

2.3.4 FEFFO for Interior Rods Adjacent to the ATRIUM Water Canister

The essential character for rods adjacent to the ATRIUM water canister is similar to the character for rods adjacent to the side (Section 2.3.2). That is, fewer rods are taken into consideration in both the numerator and the denominator of Equation 2.14. For the lower lattice of the ATRIUM-10 design, rods in the middle of the channel see three j rods and two k rods, similar to the side rods described in Section 2.3.2. Interior rods adjacent to the middle rod see three j rods and three k rods, while rods on the corner of the ATRIUM water canister see four j rods and three k rods. The calculation for FEFFO corresponding to these three cases is

$$\frac{j \quad i \quad j}{k \quad j \quad k}$$





2.3.5 Weighting Factors

The weighting factors used in Equation 2.22 of Section 2.3 determined in the work reported in Reference 2.1 continue to be appropriate and have not been modified.

2.3.6 Bundle Geometry/Spacer Effects (Additive Constants)

Spacers and bundle geometry influence the critical power behavior of the bundle. [

] These

[] are termed the Additive Constants, ℓ . Additive Constants can be considered as a flow/enthalpy redistribution characteristic for a given bundle or spacer design.



[

]

The described averaging process ensures that the ECPR (ratio of calculated critical power to measured critical power, sometimes abbreviated CPR) is always 1 for the set of experiments used to determine the Additive Constants.

Once values of $FEFF(i)$ are available, critical power can be determined on a rod-specific basis. The critical bundle power is the critical power calculated based on the limiting rod $FEFF$. The averaging process for the Additive Constants can yield values of $FEFF_{BT}$ that are lower than the limiting $FEFF$. All rods with an $FEFF(i)$ exceeding the $FEFF_{BT}$ are considered to be in boiling transition. The maximum $FEFF$ value for an assembly is determined using the Additive Constants and local peaking of the assembly. This maximum $FEFF$ may exceed the $FEFF_{BT}$ for some test sections. Using this maximum value of $FEFF$ provides an appropriate view of the mean ECPR and standard deviation characteristic of the population. The observation that some assemblies will have some rod locations where actual $FEFF$ exceeds $FEFF_{BT}$ provides for conservatism in the application of the SPCB correlation; i.e., more rods would be predicted to be in boiling transition.

2.4 ***SPCB Correlation Behavior***

The SPCB critical power correlation was investigated functionally to ensure smooth functions and no discontinuities. Section 2.4.1 describes the functional behavior of the major

components of the correlation. The correlation was also investigated for its behavior over a wide range of conditions; this is described in Section 2.4.2.

2.4.1 Functional Behavior of Major Functions Within SPCB

Functions A and B are smooth and have a weak dependence on pressure but a strong dependence on flow. Figure 2.1 and Figure 2.2 show the behavior of the A and B functions respectively. The symbols are based on pressures between 600 and 1400 psi.



Equation 2.1 shows that the function $\left[1 - \frac{B}{G}\right]$ in the correlation. This term is always positive and does not cause any discontinuity. Figure 2.3 shows the behavior of this term. The symbols in Figure 2.3 account for a range of pressures (600 - 1400 psi). [

Note that functions A and B are similar to the functions A and B described in References 2.1 and 2.2.]

2.4.2 Overall Behavior of SPCB

The critical power calculated by the SPCB correlation behaves well throughout its range of validity. This section provides results of sensitivity studies for critical power with respect to flow, pressure, inlet subcooling, FEFF, and axial power shape.



Pressure

Figures 2.6 and 2.7 show the behavior of SPCB with pressure. These figures show that pressure is only a minor contributor to critical power. The reduction in critical power with increasing pressure becomes significant at higher flow rates. [

]



Inlet Subcooling

Figures 2.8 and 2.9 show the gain in critical power with increasing subcooling reduces with a reduction in flow rate. The figures show a nearly linear impact of inlet subcooling on critical power. [

]



FEFF

The effect of FEFF on critical power is shown in Figures 2.10 and 2.11. [

]



Axial Power Profile

Figure 2.12 shows a sequence of simulated axial power profiles with peaks varying in both location and absolute magnitude. The corresponding changes in assembly critical power with respect to the variation in axial power shape are shown in Figures 2.13 and 2.14 for five different inlet flow rates. The sensitivity of critical power with respect to the variation of axial power profile is captured by the correlation through the non-uniform axial factor and through the gradient parameter. [

]

2.5 ***Additive Constants***

Additive Constants were determined using the procedure described in Section 2.3.6. These were determined for the ATRIUM-9B and for the ATRIUM-10 fuel assemblies. The verification data was used to determine the Additive Constants; the combined verification and validation data were used to determine the uncertainty of Additive Constants. The Additive Constants for

the ATRIUM-9B fuel assemblies are given in Table 3.10; those for the ATRIUM-10 are given in Table 3.11.

2.6 *Correlation Range and Applicability*

Dryout tests are performed with electrically heated test assemblies. The test assemblies have controls for power, inlet flow, pressure, and inlet subcooling. The specified test parameters are flow, pressure, and subcooling. Determining the power at which dryout occurs is the desired test result. The conditions of the test are used to determine a dryout power. The calculated dryout power divided by the measured power defines the ECPR. In addition, the calculation determines fluid conditions at every location of the bundle.

2.6.1 Mass Velocity

The range of applicability for nodal mass velocity at the plane of boiling transition is presented in Table 1.2. [

]

2.6.1.1 Steady-State Core Monitoring

High Mass Velocity Limit

If the nodal mass velocity exceeds the high mass velocity applicability limit, an overly optimistic critical heat flux for the node might be predicted because of using the correlation beyond its test range. To avoid this situation and to provide a conservative estimate of the bundle critical power ratio, assemblies with mass velocities greater than the high mass velocity limit are analyzed with the mass velocity conservatively reduced to the high mass velocity limit. This results in conservatively high enthalpy and quality distributions in the bundle and the use of the SPCB correlation within its range of applicability to produce a conservative CHF and bundle critical power ratio (CPR).

Low Mass Velocity Limit

The critical power calculation is not performed for a bundle with a nodal mass velocity below the low mass velocity applicability limit. Appropriate messages are printed in calculational output.

2.6.1.2 Transient Δ CPR Analysis

The Δ CPR during a transient is the difference between the steady-state CPR before the transient and the minimum CPR during the transient. The transient calculation is performed with an initial assembly power that results in boiling transition (critical heat flux ratio = 1.0) at the worst point throughout the transient simulation. The computer program checks the coolant conditions at the time of boiling transition against the SPCB applicability limits.

High Mass Velocity Limit

If the nodal mass velocity exceeds the high mass velocity limit at the worst point in the transient, CHF is calculated with both the actual nodal mass velocity, and again with the nodal mass velocity set to the critical power correlation high mass velocity limit. The transient CHF is determined from the more conservative of the two calculations.

Low Mass Velocity Limit

If the nodal mass velocity is below the low mass velocity limit at the point of boiling transition, the transient CHF is determined from the Hench-Levy correlation (Reference 2.8).

2.6.1.3 MCPR Safety Limit

High Mass Velocity Limit

The same logic that is applied in the steady-state core monitoring is used for the minimum critical heat flux ratio (MCHFR) node in the MCPR safety limit calculation. The difference is that the resultant lower CHF is used to determine the number of rods in boiling transition rather than the bundle CPR.

Low Mass Velocity Limit

If the MCHFR nodal mass velocity is below the low mass velocity limit, every rod in the bundle is assumed to be in boiling transition.

2.6.2 Enthalpy

The range of applicability for nodal enthalpy at the plane of boiling transition is presented in Table 1.2 as a function of nodal mass velocity. These ranges represent the boiling transition enthalpies envelope observed during SPC testing. Because the boiling transition enthalpy is a primary hydraulic parameter that characterizes the bundle CHF performance for the current hydraulic conditions and the neutronic power distribution within the bundle, specific checks are made within the SPC methodology for exceeding these limits.

2.6.2.1 Steady-state Core Monitoring

High Enthalpy Limit

If the boiling transition nodal enthalpy exceeds the high enthalpy applicability limit, dryout is assumed to occur when the bundle power is elevated to produce the boiling transition nodal enthalpy equal to the high enthalpy applicability limit. Even though the SPCB correlation used at the high enthalpy applicability limit would predict margin to dryout, no credit is taken and the CPR is limited by the high enthalpy applicability limit.

Low Enthalpy Limit

If the boiling transition nodal enthalpy is below the low enthalpy applicability limit, the bundle enthalpy and corresponding quality distributions are artificially increased to compute a CHF corresponding to a boiling transition nodal enthalpy within the correlation applicability limits. Because CHF decreases with increasing enthalpy, this results in a conservative CHF based on the use of the SPCB correlation within its range of applicability. This CHF is then used in the critical power calculation for the bundle.

2.6.2.2 Transient Δ CPR Analysis

High Enthalpy Limit

If the boiling transition nodal enthalpy exceeds the high enthalpy applicability limit, the transient simulation is repeated with a lower radial power factor (higher initial critical power ratio) until the worst point in the transient results in a nodal enthalpy below the high enthalpy limit. This treatment results in a conservative transient simulation because the hot bundle will not experience boiling transition (i.e., minimum critical heat flux ratio > 1.0) and the SPCB correlation is applied within its range of applicability.

Low Enthalpy Limit

If the boiling transition nodal enthalpy is below the low enthalpy applicability limit, the transient CHF is determined from the Hensch-Levy correlation (Reference 2.8) provided the calculated CHF from Hensch-Levy is greater than the calculated CHF from the SPCB correlation; otherwise, the bundle enthalpy and the corresponding quality distributions are artificially increased to compute a CHF corresponding to a boiling transition nodal enthalpy that is within the correlation applicability limits. Because CHF decreases with increasing enthalpy, this results in a conservative CHF, which is based on the use of the critical power correlation within its range of applicability.

2.6.2.3 Safety Limit

High Enthalpy Limit

If the MCHFR nodal enthalpy is above the high enthalpy limit, every rod in the bundle is assumed to be in boiling transition.

Low Enthalpy Limit

If the MCHFR nodal enthalpy is below the low enthalpy limit, the enthalpy and quality distributions are artificially increased, as in the steady-state core monitoring calculation to determine a conservative CHF. This CHF is then used to compute the number of rods in boiling transition.

2.6.3 Pressure

The range of applicability for pressure is presented in Table 1.1. If the pressure falls outside this range, appropriate messages are printed and the calculation is stopped.

2.6.4 Inlet Subcooling

The test range for inlet subcooling is presented in Table 1.1. The SPC methodology checks the inlet subcooling against this range; if the subcooling falls below the test range minimum, the calculation is stopped. If the subcooling exceeds the test range maximum, the inlet subcooling is set to the maximum subcooling limit.

2.7 ***SPCB Application to Other Fuel Designs***

The SPCB Critical Power Correlation performs well for the ATRIUM-9B and ATRIUM-10 fuel designs. The SPCB correlation may also be applicable to other vendor fuel designs or future SPC fuel designs which have design changes influencing the critical power characteristics. The performance of the SPC correlation for other vendors' fuel designs or future SPC fuel designs with different critical power performance requires appropriate assessment, determination of uncertainties, and determination of boundaries. With sufficient measured data, including a broad range of flows, pressures, subcoolings, axial power shapes, and local peaking configurations, the process used for determining Additive Constants for the ATRIUM-9B or ATRIUM-10 fuel can be directly applied.

With data that are calculated based on an alternative critical power correlation, then the process described in Reference 2.6 for ANFB and submitted as one generic process in Reference 2.7 could be used to obtain appropriate characterization. The use of the generic process in Reference 2.7 requires the use of the appropriate ratio of ECPR standard deviation to Additive Constant standard deviation. [

]

2.8 ***References***

- 2.1 EMF-1997(P)(A) and Supplement 1, *ANFB-10 Critical Power Correlation*, Siemens Power Corporation, July 1998.
- 2.2 ANF-1125(P)(A) and Supplements 1 and 2, *ANFB Critical Power Correlation*, Advanced Nuclear Fuels Corporation, April 1990.

- 2.3 L. S. Tong, et al., "Influence of Axially Non-Uniform Heat Flux on DNB," Chemical Engineering Progress Symposium Series, No. 64, V 62, 1966.
- 2.4 J. G. Collier, *Convective Boiling & Condensation*, Second Edition, McGraw Hill, 1981.
- 2.5 R. T. Lahey, Jr. and F.J. Moody, *The Thermal Hydraulics of A Boiling Water Nuclear Reactor*, Second Edition, ANS Monograph, 1993.
- 2.6 EMF-1125(P)(A) Supplement 1, Appendix C, *ANFB Critical Power Correlation Application for Co-Resident Fuel*, Siemens Power Corporation, August 1997.
- 2.7 EMF-2245(P), *Critical Power Correlation Application for Co-Resident Fuel*, Siemens Power Corporation, July 1999.
- 2.8 NRC-IC-99-022, *Modifications to Procedures for Use of XCOBRA-T*, June 10, 1999.

3. Statistical Analysis of SPCB Critical Power Data

The SPCB data statistics discussed in this section include descriptive statistics for the data set, an evaluation of the distribution characteristics, figures of ECPR with respect to correlation parameters, and descriptive statistics for Additive Constants and Additive Constant Uncertainty.

The next section addresses the validation data separately from the combined data.

3.1 *SPCB Descriptive Statistics*

Table 3.1 shows the mean ECPR, standard deviation of the mean and number of data by test section. Additional information in the table includes the fuel design represented (ATRIUM-9B or ATRIUM-10) and the axial power shape represented (Cosine, Downskew, or Upskew).



Higher moments for the SPCB analysis of ECPR are computed and results are presented for the following equations. Reference 3.1 provides the relationships for computing the higher order moments. These higher order moments include the third moment about the mean and the fourth moment about the mean and are given by

$$m_3 = \frac{\sum_{i=1}^n (x_i - \bar{x})^3}{n}$$

Third moment about mean

$$m_4 = \frac{\sum_{i=1}^n (x_i - \bar{x})^4}{n}$$

Fourth moment about mean

Similarly, the second moment is given by

$$m_2 = \frac{\sum_{i=1}^n (x_i - \bar{x})^2}{n}$$

Second moment about mean

A measure of skewness is given by:

$$\sqrt{\beta_1} = \frac{m_3}{m_2^{1.5}}$$

Skewness measure

A measure of kurtosis is given by

$$\beta_2 = \frac{m_4}{(m_2)^2}$$

Kurtosis measure

The values of the measures with respect to ECPR are

$$\begin{aligned} m_2 &= 0.000491 \\ m_3 &= 0.000000 \\ m_4 &= 0.000000680450 \\ \sqrt{\beta_1} &= 0.004488 \\ \beta_2 &= 2.83 \end{aligned}$$

These statistics are close to those of a normal distribution. The distributional character of the SPCB critical power ratios are viewed in Figures 3.1 and 3.2. Figure 3.1 is a histogram of the frequency of occurrence of CPR while Figure 3.2 shows that the distribution generally follows the linear characteristics of a normal distribution. As is shown later, the correlation over predicts the number of rods in boiling transition. The behavior of the CPR distribution is adequately represented by normal distribution characteristics for the safety limit analysis.





3.2 ***Statistical Tests***

The SPCB data were tested using Lilliefors test for normality (Reference 3.2). The test indicates that at the one percent significance level the assumption of normality cannot be rejected.

3.3 ***SPCB Correlation Behavior***

Figures 3.3 through 3.8 show the SPCB ECPR values graphically with respect to mass flow rate, boiling transition enthalpy, pressure, FEFF, and other parameters.





3.4 *Statistics by Subgroups*

The descriptive statistics for the overall data can be examined by several subgroups of data. Mean, standard deviation, and number of data are presented. This section covers all data. Validation data is separated out in Section 4.

3.4.1 Mass Flow Rate

Table 3.3 shows the results of examining representative mass flow rate groups from []



3.4.3 Enthalpy at Boiling Transition

Table 3.5 shows the results of examining representative boiling transition enthalpies from [].



3.4.5 Axial Offset

Table 3.7 gives the results of examining representative axial offset values.





3.4.7 Mass Flow Rate and Enthalpy Groups

Characteristics for the SPCB ECPR can be examined by considering data within different ranges of flow and inlet subcooling. Table 3.9 shows this characterization based on eleven flow groups and three inlet subcooling ranges.



3.5 *ECPR - Mass Flow Plots*

The overall view of ECPR versus mass flow is shown in Figure 3.3 and no trend is observed. Figures 3.8 through 3.35 show the behavior of ECPR with mass flow for each test section. Within individual tests, some tests over predict high flow and some under predict high flow. Because the evaluations are performed using the FEFF calculated for the test section based on the composite Additive Constants, some test sections provide under predictions for many flows. Figure 3.36 shows the combined behavior of ECPR with mass flow for the upskew data.

Pages 3-15 through 3-28 are proprietary in toto.

3.6 ***Additive Constant Statistics***

The Additive Constants for the ATRIUM-9B and ATRIUM-10 fuel designs were developed using the process summarized in Section 2. This section presents the determination of the Additive Constants and uncertainty and describes the conservatism for the SPCB critical power correlation. Tables 3.10 and 3.11 provide the Additive Constants for the ATRIUM-9B and ATRIUM-10 fuel designs.

3.6.1 Additive Constant Determination

The steps summarized in Section 2.3.6 are provided here in more detail.

Step 1: Identify Rods in Boiling Transition

[

]



Step 2: Determine FEFFBT for each Data of Interest

[

]

[

]

[

]

Step 3-6: Additive Constant Determination

[

]

The results of evaluating the Additive Constants for use with the ATRIUM-9B and ATRIUM-10 fuel designs are presented in Tables 3.10 and 3.11.

3.6.2 Additive Constant Uncertainty

Determining Additive Constants Uncertainty provides for combining the standard deviations of the FEFFBT using a propagation of error method. This process employs the approach used for ANFB. Two major factors contribute to the overall uncertainty of the Additive Constants. These are 1) within test variability and 2) between test variability. The process includes contributions from the cosine axial tests and the upskew/downskew axial tests. The propagation of error method used is implemented by taking the square root of the sum of the squares of the errors. Errors in determining the uncertainty of the Additive Constants include the standard deviation of the FEFFBT for each test section and the difference between a specific value of FEFFBT and FEFF for a rod observed in boiling transition. Weighting factors of the number of rods observed in boiling transition and the number of tests are incorporated

into the process to determine the total standard deviation of the Additive Constants.

Specifically, where

N	=	Number of test bundles
M	=	Number of rods in these test bundles
FEFFBT	=	Best estimate FEFF for bundle
DFBT(i)	=	Standard deviation of FEFFBT for test bundle i
NOEX(i)	=	Number of experiments with test bundle i
NBT(J,i)	=	Number of boiling transition detected on rod j of test bundle i
DELTA(J,i)	=	Difference between FEFFBT and FEFF of rod j observed in boiling transition in test bundle i
DELTEX	=	Total standard deviation in Additive Constants
NTOT	=	Total number of experiments for all tests
NBTOT	=	Total number of rods in boiling transition

The Additive Constant uncertainty is calculated using



Evaluating the ATRIUM-9B data based on the verification data statistics (shown in Table 3.13) results in an Additive Constant uncertainty of [] for the ATRIUM-9B. Similarly the evaluation of the ATRIUM-10 data based on the verification data statistics results in an Additive Constant uncertainty of [] for the ATRIUM-10. The impact of the validation data needs to be included. This is accomplished by evaluating the validation data set for its FEFF values for each validation data point, then including the values in the mean and standard deviation of FEFF for each test section. To maintain a single process between ATRIUM-9B and ATRIUM-10, this process is chosen rather than using a replicate point process as was used for the ANFB-10 correlation.



Using the values of composite values FEFFBT and Standard Deviation of FEFFBT (Table 3.14) for the respective fuel designs, the overall uncertainty for Additive Constants is determined to be []

3.6.3 High Local Peaking

A series of dryout tests were performed on the ATRIUM-9B and the ATRIUM-10 to determine the effect of high local peaking on the Additive Constant methodology. Because of physical manufacturing limits on the test section heater rods, the highest local peaking attained was 1.45. The axial power profile for the test assembly was 1.4 peak to average cosine.

[

]





The Additive Constant uncertainties determined by the Additive Constant methodology are
[] While this conclusion may be drawn from examining the plots, a statistical analysis provides a more rigorous process for demonstrating this. Therefore, a Bartlett test (Reference 3.3, page 802) was applied based on data for each test over the same range of test conditions. The Bartlett test considers the null hypothesis that the variance of each data set is an estimate of the same population variance. The result of this test affirms that the null hypothesis cannot be rejected.

[

]

The uncertainty used for rods peaked greater than 1.5 is then determined by the square root of the sum of the squares of the Additive Constant uncertainty and its respective incremental uncertainty. This is the same method used in the approved ANFB-10 methodology (Reference 3.4).

3.6.4 SPCB Conservatism

The Additive Constants for the ATRIUM-9B and ATRIUM-10 designs are applied to the local peaking patterns for the test assemblies [

]

[

] A further measure of the conservatism of the SPCB correlation is observed by comparing the FEFF values for the assembly with the FEFFBT that places the ECPR of the assembly at 1.0. This allows the determination of the number of rods calculated to be in boiling transition for each data of each test section. Comparing the calculated number of rods in boiling transition with the number of rods in boiling transition, an over estimate of the number of rods in boiling transition is determined. The ratio of the number of rods calculated to be in boiling transition to the number of rods observed to be in boiling transition is equal to [] when using the SPCB critical power correlation.

3.7 *SPCB Predictions Compared with Measurements*

The predicted values of critical power are compared with the measured values and presented in Figure 3.39.

3.8 **References**

- 3.1 G. J. Hahn, S. S. Shapiro, *Statistical Models in Engineering*, Wiley, 1967.
- 3.2 H. W. Lilliefors, *On the Kolmogorov-Smirnov Test for Normality with Mean and Variance Unknown*, Journal of the American Statistical Association, Vol. 62, June 1967.
- 3.3 *Statistical Methods for Nuclear Material Management*, NUREG/CR4604, PNL-5849, December 1988.
- 3.4 EMF-1997(P)(A) and Supplement 1, *ANFB-10 Critical Power Correlation*, Siemens Power Corporation, July 1998.

4. Correlation Validation

The development of the SPCB correlation required that the data base be divided into two sets, one for correlation development and the other for correlation validation. When the correlation development was complete, the correlating data set was used to verify that the correlation had a proper fit to the data. In this context, the data set used for correlation development is termed the verification set.

The process for validating the SPCB critical power correlation contains several steps. In accordance with the criteria set forth in Reference 4.1, 20 percent of the data was set aside and defined to be a validating set of data. The remaining 80 percent was used to develop the critical power correlation. In addition, data acquired during the correlation development process was used only for validation. Further, data obtained for an assembly design that [

] was used only for validation. The SPCB critical power correlation was further validated by comparing its prediction with the measurements made for transient critical power tests.

4.1 *Assessment of ATRIUM-9B/ATRIUM-10 Critical Power Data*

Information presented in Section 3 provided a combined characteristic for the SPCB correlation based on the evaluation of the verification and validation data base for the ATRIUM-9B and ATRIUM-10 fuels. Specific evaluation showed that the Additive Constant uncertainties were unchanged when the entire data base was considered versus when only the verification data base was considered. This section intentionally examines the validation data base.

4.1.1 Comparison of ATRIUM-9B Verification and Validation Data

The statistical comparison of the ATRIUM-9B verification and validation data sets is presented in Table 4.1.

Graphically, the predicted versus measured critical power for ATRIUM-9 Validation data is shown in Figure 4.1.

While the behavior of the ECPR with flow is shown in Figure 4.2.



4.1.2 Comparison ATRIUM-10 Verification and Validation Data

The statistical comparison of the ATRIUM-10 verification and validation data sets is presented in Table 4.3.





The behavior of ECPR vs Flow is shown in Figure 4.4.



4.2 *Validation with Alternate Design*

The SPCB critical power correlation is further validated by evaluating the critical power performance for [

] The characteristic swirl vanes of the ATRIUM-10 are incorporated on the spacer design used in the validation test and the rod diameter is identical to the ATRIUM-10 design. The ATRIUM (central water canister) remains in the same position. Part-length rod positions differ in the ATRIUM-10 with [

] rods and the ATRIUM-10P with [

] All part-length rods occur one row in from the channel. The data set contains 316 data points. The result of the tests shows that the mean ECPR is [

] Figure 4.5 shows the predicted versus measured critical power for these tests. Figure 4.6 is an example of one of the test assembly's critical power versus subcooling plots.





4.3 *Evaluation of Transient Critical Power Data*

An industry-accepted standard in BWR transient methodology is that steady-state dryout correlations are appropriate to use in transient methodology. Transient dryout tests with cosine and upskew profiles were performed to reconfirm this for the ATRIUM-10 when using the SPCB critical power correlation.

The ATRIUM-10 [] transient critical power tests were performed for test assembly 17.8 (cosine power shape), test 29.5 (upskew axial power shape), and 48.1 (upskew axial power shape). Thirty-two transient tests were evaluated: [] For comparison, the steady-state performance of the ATRIUM-10 as measured and as predicted by SPCB is given in Figure 4.7. The SPCB correlation correlates well with the respective tests.

[

]

The transient tests of interest are both simulated load rejection without bypass (LRNB) events that consist of power and pressure ramps and flow decay; and simulated pump trip events that consist of flow decay and power decay. The flow, pressure, and power are controlled by a function generator. The forcing functions were programmed to produce the transient rod surface heat flux typical of the various events. Figure 4.8 shows the forcing function characteristics for a typical LRNB test while Figure 4.9 shows the comparable forcing function characteristics for a typical pump trip event.





Figure 4.10 illustrates the response of thermocouples attached to the interior of the heater rod tubing. Initially, the clad temperature rises in response to the pressure and power ramps. The transition point, where the heat transfer mode changes from nucleate to film boiling, is characterized by a sudden, rapid increase in clad temperature. This point defines the onset of boiling transition and shows that boiling transition has occurred. Boiling transition occurs slightly upstream of [] In the STS-17.8 tests, boiling transition normally occurred [] In the STS-29.5 and 48.1 tests, it occurred []



Parameters monitored during the tests include power, inlet flow, system pressure, inlet temperature, [

]

The SPC transient thermal hydraulic code XCOBRA-T (References 4.2 and 4.3), is used to predict the transient test results using the SPCB steady-state critical power correlation. XCOBRA-T calculated the fluid conditions axially at time steps as small as []. The test power forcing function provides the boundary condition of power, which appears immediately as heat flux (i.e., no time delay) from the surface of the rods. The CHF is calculated at each axial position and time step, then compared to the corresponding rod heat flux. The ratio of the critical heat flux to the rod heat flux is CHFR. A MCHFR of unity during the transient signifies boiling transition. Although applying the steady-state critical power correlation is considered conservative, SPCB is a best fit correlation, and for a given steady-state condition shown to be in boiling transition by test, the correlation may under- or overpredict a boiling transition state within the range of defined uncertainties. Thus, during

transient test conditions, dryout may not be predicted for all cases because of the defined uncertainties.

Thirty-two transient tests modeling the ATRIUM-10 geometry in simulated LRNB or pump-trip events were evaluated. The two STS-17.8 tests had nearly the same forcing functions, with only the initial power level differing. The nine STS-29.5 tests consisted of six 100 percent flow cases and three 80 percent flow cases. Within these groups, there was a variation in inlet subcooling. The 21 STS-48.1 tests consisted of nine LRNB tests with five LRNB at 100 percent flow and four LRNB tests at 80 percent flow, and 12 pump-trip tests. The 12 pump-trip tests included eight at 100 percent flow and four at 80 percent initial flow. The initial subcooling varied among these tests. Table 4.4 summarizes initial state conditions for all the transient tests.

* At elevation of minimum CHF.

The XCOBRA-T calculations were performed using nominal Additive Constants. The results using nominal (design) Additive Constants are summarized in Table 4.5. Figure 4.11 compares the measured and calculated time of boiling transition. The comparisons demonstrate that the STS-17.8, STS-29.5 and STS-48.1 transient tests are conservatively predicted. These results validate that Additive Constants can be derived from steady-state tests and applied to transient conditions.

* XCOBRA-T time of BT occurs when CHFR is 1.0.

4.3.1 Conclusions

The XCOBRA-T analyses calculated dryout in the [] evaluated at nominal design conditions. When considering uncertainties, all transient results were conservatively predicted. This validation confirms that the use of the SPCB steady-state dryout correlation is appropriate for use in evaluation of transient events. Furthermore, this evaluation provides a validation that Additive Constants can be derived from steady-state tests and applied to transient conditions.

4.4 **References**

- 4.1 EMF-2022, Revision 0, *Correlation Development Guideline*, Siemens Power Corporation, February 1998.
- 4.2 XN-NF-84-105(P)(A) Volume 1 and Volume 1 Supplements 1 and 2, *XCOBRA-T: A Computer Code for BWR Transient Thermal-Hydraulic Core Analysis*," Exxon Nuclear Company, February 1987.
- 4.3 XN-NF-84-105(P)(A) Volume 1 Supplement 4, *XCOBRA-T: A Computer Code for BWR Transient Thermal-Hydraulic Core Analysis Void Fraction Model Comparison to Experimental Data*, Advanced Nuclear Fuels Corporation, June 1988.

5. SPCB Data Base

The SPCB data base contains [

] to validate the correlation. All data was taken at the Siemens test facility at Karlstein, Germany.

5.1 Facility Description

All dryout testing for the ATRIUM-9B and ATRIUM-10 assembly was performed at the Siemens thermal hydraulic test loop at Karlstein, Germany. Figure 5.1 shows that the thermal hydraulic test facility is a high-pressure-water heat-transfer loop containing a test vessel, as shown in Figure 5.2, with the test bundle and upper and lower bus bars, high-pressure coolers, a direct-contact condenser, a pressurizer, and the main circulation pumps. The test loop is rated at 2683 psi and 680°F. The DC power supply consists of four thyristor controlled rectifier models, each rated at 20,750 amps, with a design power of 15 MW.

The data acquisition system uses a DATA GENERAL MV 7800 computer to sample the analog signals of the loop instrumentation, digitize them, and store the signals on hard disc. The system has 176 channels available and a sample rate of 20 samples per second and channel. After the test, the data is archived on magnetic tapes. Table 5.1 shows the test loop uncertainties.

During the dryout test, the dryout power is determined manually when the temperature of a heater rod thermocouple rises more than [] Additionally, after the test, the data obtained from each thermocouple is evaluated to determine the maximum value. The point of data evaluation for critical power is considered to be between 24.6 seconds and 34.2 seconds of the total file record. Dryout is defined to have occurred if the maximum value of the thermocouple reading is more than [] than the arithmetic mean value of the first five temperature values from the beginning of the defined time window. If a thermocouple has an increase in temperature of greater than [] the thermocouple is defined as defective and excluded from data evaluation.

Using the time of dryout defined from the thermocouple evaluation, the arithmetic mean values of 11 consecutive power measurements are determined. The maximum mean is defined as the critical power.

5.2 *Test Bundle Descriptions*

The dryout test bundles are full array assemblies designed to represent the production fuel assembly as close as possible. The rod bundle is housed in a ceramic liner fabricated from alumina ceramic with a purity of 99 percent or better. The inner dimension of the liner is 5.276 in. with the corners rounded to a radius of 0.39 in. The liner serves to simulate the flow channel and electrically insulate the spacers from each other. The ceramics are housed in a stainless steel outer channel assembly.

The heater rods used in the testing are direct heaters; that is, the current flowing through the rod wall provides the heating. Therefore, the thickness of the heater wall determines the relative power of the rod and the variation in wall thickness determines the axial power profile. The high-powered rods, where critical heat flux is expected to occur, are equipped with thermocouples for dryout detection (see Figure 5.3). The thermocouples are located radially to point to the subchannel of interest and axially about 0.5 in. below the top three spacers of the active length.

5.2.1 ATRIUM-9B

The ATRIUM-9B test bundle consists of a square array of rods supported at fixed axial locations by ULTRAFLOW spacers and with one 1.516 in. square cross-section water channel. The array contains 72 full-length rods.

The test bundles have the following characteristics (Table 5.2 summarizes the physical characteristics of the ATRIUM-9B test assembly).

[

]

[

]

Three axial power profiles were tested during the ATRIUM-9B dryout test series. The STS-12, STS-33, STS-37, and STS-40 series were performed on a [] peak-to-average chopped cosine axial, the STS-35 series was [] peak-to-average downskew axial, and the STS-35 and STS-38 series was performed on a [] peak-to-average upskew axial power profile. Figure 5.5 represents the rod axial power profiles.

5.2.2 ATRIUM-10

The ATRIUM-10 test bundle consists of a square array of rods supported at fixed axial locations by ULTRAFLOW spacers and with one 1.378 inch square cross section water channel. The array contains 83 full length rods and 8 part length rods.

The test bundles had the following characteristics: (Table 5.3 summarizes the physical characteristics of the ATRIUM-10 test assembly).

[

]

During testing, the test bundle is shimmed to its most conservative lateral position by placing shims on the top three spacers.

Three axial power profiles were tested during the ATRIUM-10 dryout test series. The STS-17 and STS 32 series were performed on a [] peak to average chopped cosine axial, the STS-28 series was [] peak to average downskew axial, and the STS-29 series was performed on a [] peak to average upskew axial power profile. Figure 5.5 represents the rod axial power profiles. For the part length rods, the axial power shape is the same as a full length rod, except that is it truncated at the end of the part length rod.

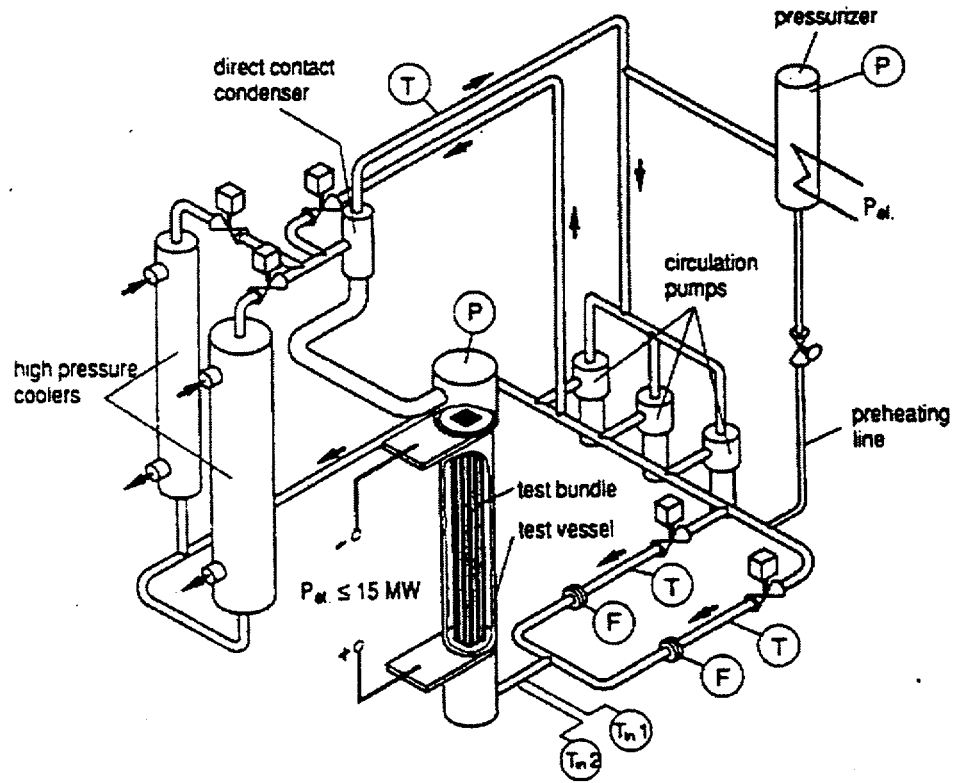


Figure 5.1 Karlstein Thermal Hydraulic Test Loop

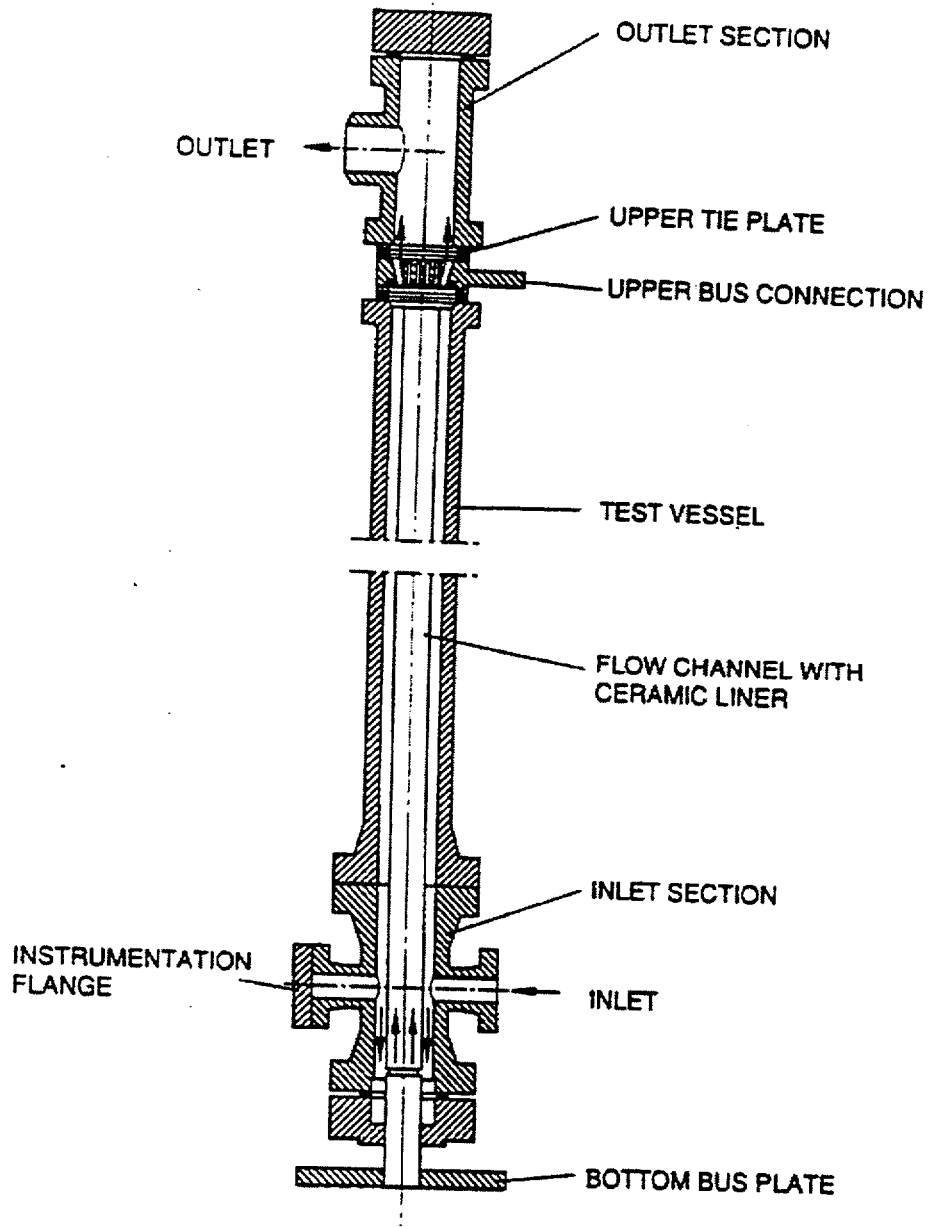


Figure 5.2 Test Vessel









5.3 Test Strategy

The development of a dryout correlation requires the acquisition of an appropriate data base, where an appropriate data base is defined as one that fills the applicable domain with acceptable density, displays acceptable uncertainty everywhere, and provides repeatability. This presents a particular challenge for dryout correlation development. Radial peaking, axial power profile, pressure, flow, and inlet subcooling have been considered in developing the testing strategy to ensure that the number of assemblies used in the correlation is sufficient.

5.3.1 Radial Peaking Profiles

A conservative assumption is made in the SPC dryout methodology that any rod position in which a symmetric rod is not driven into dryout is assumed to have been in dryout at its highest local peaking. The usual practice is for the local peaking of the test rods to vary between 0.9 and 1.2, with peaking as low as 0.6 used occasionally. Because the purpose of the variation in local peaking is to determine the dryout characteristics of a particular rod position, no effort is made to simulate any particular neutronic design.

The testing program takes advantage of the symmetry of the test bundle. The ATRIUM-9B bundle has octant symmetry, so that peaking nine individual rods of twelve symmetric positions with five driven into dryout adequately describes the assembly. The rod positions tested were the corner rods, the peripheral rods, the rods in the middle row, and the rods around the internal water canister. The ATRIUM-10 has half-bundle symmetry along the diagonal of the bundle. In all, [] All major positions of the fuel assembly were tested.

Specific tests were performed during the testing of the ATRIUM-10 assembly to demonstrate the effect of radial peaking on Additive Constants. The test series STS-17.5 and STS-17.6 peaked rod [] respectively. Then STS-32.1 was performed to peak rod [] With the completion of these tests, the representative locations in the bundle were driven into dryout at different local peaking factors. To demonstrate that the ATRIUM-9B bundle behaves the same, two tests were run at the same location with a local peaking factor of [] Only two tests needed to be performed on the ATRIUM-9B because the purpose was to demonstrate that the

algorithm for the Additive Constant methodology behaved the same for the ATRIUM-9B as for the ATRIUM-10. Section 3.1 of this report documents the statistical results of these tests.

5.3.2 Axial Power Profile

Three axial power profiles were tested during dryout testing: [] peak to average cosine, [] peak to average upskew, and [] peak to average downskew (see Figure 5.5). Because cosine power shapes are representative of much of the plant operation they are the most prevalent type of testing; other axial power profiles are used to check the axial power corrector used. Dryout occurs only after the peak of an axial power profile. For the ATRIUM-9 and ATRIUM-10, upskew axial power shapes dryout occurs only under the topmost spacer of the heated length. For a cosine axial power shape, dryout may occur under the top or second from the top spacer of the heated length. The same happens for a downskew axial power shape for a fully rodded bundle; for the ATRIUM-10 the dryout may occur as low as the third spacer from the top. For any fuel assembly, the upskew axial power profile will have less critical power than the cosine axial power shape for the same local peaking, and the downskew axial power shape will have higher critical power than the cosine. In general, for the same peak-to-average power shape, for a fully rodded bundle the increase in critical power of a downskew axial will be about the same as the loss of critical power for the upskew relative to the cosine axial power shape.

The ANFB (Reference 5.1) correlation was developed using uniform axial power data, then the axial power corrector was developed using cosine and upskew data. A uniform axial power profile always results in dryout occurring at the exit of the bundle, and, therefore, would easily provide accurate data on the enthalpy at the plane of boiling transition. Because uniform axial power profile rods were not available for the ATRIUM-9B and ATRIUM-10 assemblies and the manufacture of those rods requires a long lead time, the SPCB was developed by calculating the enthalpy at the plane of boiling transition of each individual case.

5.3.3 Thermal Hydraulic Test Conditions

The data base for the ATRIUM-10 was obtained during the ANFB-10 correlation development (Reference 5.2). It contains data over a range of [] a subcooling of [] and pressures ranging from [] The ATRIUM-9B originally had 125 data points taken over a range of 0.05 Mlb/hr to 0.15 Mlb/hr, a subcooling of 8 Btu/lbm to 90 Btu/lbm at a system pressure of 1000 psia. This database was expanded to include the full range of pressures and flows. Table 5.4 summarizes the tests and test conditions used in the development, verification, and validation of the SPCB correlation.

5.3.4 Test Design

The methodology developed for performing dryout testing is fairly standard. The testing is performed by setting pressure and flow. The inlet subcooling is then set and the power is slowly increased until dryout is achieved. The inlet subcooling is then decreased or increased and the process is repeated. After one flow condition is tested, the flow is reset to the desired rate and the entire process is repeated. After all inlet subcoolings and flows are tested, the pressure may be changed and testing continued. To ensure that this did not introduce a systematic error, the test process was changed for a few points. In this change, the flow and

power were held constant and the inlet subcooling varied until dryout was reached. This process reproduced the standard test procedure.

Because the dryout test results are somewhat ordered, most errors in the test are immediately evident. When the flow is set, the critical power will vary directly with the inlet subcooling. The slope of the line increases as the flow increases. This may be seen in any of the plots at the end of this section. During the test series for each day, some test points are repeated to ensure reproducibility.

The development of the test plan is dependent on the use of the data. For example, for the validation test, STS-38.3, a test plan as developed in Reference 5.1 was used. Because of the small amount of data available for the ATRIUM-9B, the testing performed for the SPCB correlation included all pressures and flows. Because the data base for the ATRIUM-10 was larger, not only did some tests have all pressures and flows, statistical design of experiments was also used (Reference 5.2).

5.4 *SPCB Data*

The data base for SPCB contains [] peaking patterns performed on test sections with cosine, upskew, and downskew axial power profiles for ATRIUM-9B and ATRIUM-10 designs. The correlation data base contains [] data points taken over the range of applicability of the SPCB correlation. Of the [] data points, [] form the information used during the correlation process and [] data points validate the correlation. Table 5.5 contains the measured and calculated critical power ratio of the verification and validation data base. Figures 5.6 through 5.89 present the dryout test peaking pattern and its associated inlet subcooling versus critical power plot for both the test data and the SPCB prediction of the test data.

Pages 5-15 through 5-168 are proprietary in toto.

5.5 **References**

- 5.1 ANF-1125(P)(A), *ANFB Critical Power Correlation*, Advanced Nuclear Fuels Corporation, April 1990.
- 5.2 EMF-1997(P)(A), *ANFB-10 Critical Power Correlation*, Siemens Power Corporation, October 1998.

Distribution

Richland Distribution (e-mail only)

Safety Analysis Methods
BWR Safety Analysis
BWR Neutronics
Neutronic Analysis Methods
R. L. Feuerbacher
R. S. Reynolds
Customer Projects
J. S. Holm
C. M. Powers

Richland Distribution

H. D. Curet (1 + 15 for NRC)
T. H. Keheley (1)
R. B. Macduff (1)
A.L.B. Ho (10 for Taiwan)
D. E. Garber (2)
K. V. Walters (6)

Erlangen Distribution (e-mail only)

Dr. R. Huq
P. Knabe
Dr. W. Uebelhack
Dr. R. Zimmermann